

RESEARCH

Open Access



# $\beta$ -cyclodextrin cross-linked metal organic frameworks as a new sensing candidate for donepezil hydrochloride potentiometric sensors

Rehab O. El-Attar<sup>1\*</sup>, Reda M. Abdelhameed<sup>2</sup> and Elmorsy Khaled<sup>1</sup>

## Abstract

Screen-printing is a well-established promising technology for large scale production of planner disposable electrochemical sensors. The present study aims to fabricate a novel donepezil hydrochloride (DPH) screen-printed sensor integrated with the cross-linked  $\beta$ -cyclodextrin-functionalized aluminum metal organic framework-multiwall carbon nanotubes nanocomposites ( $\beta$ -CD/MOF/MWCNTs) as a novel sensing element. The fabricated disposable sensors exhibit theoretical Nernstian compliance value of  $60.7 \pm 1.5$  mV decade<sup>-1</sup> within a linear dynamic concentration range from  $10^{-6}$  to  $10^{-2}$  mol L<sup>-1</sup> and limit of detection  $7.0 \times 10^{-7}$  mol L<sup>-1</sup>. The DPH disposable sensors show high potential stability with a prolonged operational lifetime and the fast response time of 6 s. The presented electrochemical sensors represent an efficient analytical tool for fast and sensitive assay of DPH residues in the marketed pharmaceutical tablets and biological samples with acceptable average recoveries under direct potentiometric measurements, flow injection analysis (FIA), and potentiometric titration. Moreover, the dissolution and degradation studies of DPH can be monitored by the presented disposable sensors.

**Keywords** Donepezil hydrochloride, Planner disposable sensors,  $\beta$ -cyclodextrin cross-linked metal–organic frameworks, Pharmaceutical analysis, Biological samples, Dissolution studies

## Introduction

Based on their high surface/volume ratio, nanomaterials brought challenging and promising opportunities for developing the analytical performance of electrochemical sensors [1–6]. Recently, the progress in the synthesis of crystalline porous materials found tremendous attention, where metal–organic framework (MOF)

represents a new member in the vast field of porous three-dimensional coordination materials combining the advantages of both organic and inorganic materials [7, 8]. The organic linkers, central metal ions, and sequentially structural motifs yield infinite possibilities of MOF structures and combinations [9–12]. The functionalized MOFs can be cross-linked with various macromolecules with tunable properties and the synergic effect of both components. Post synthesis modification of MOFs with cyclodextrins (CDs) and other macrocyclic compounds assures synergistic performance of both the nanostructure of MOFs and the inclusion complex formation of CDs with the target analyte [13–19]. Therefore, MOFs regarded as promising candidates for drug delivery, gas sorption, ion exchange, photocatalysis, separation, water

\*Correspondence:

Rehab O. El-Attar  
rhbattar@yahoo.com

<sup>1</sup> Microanalysis Laboratory, Applied Organic Chemistry Department, National Research Centre, El Bohouth St., Dokki, Giza 12622, Egypt

<sup>2</sup> Applied Organic Chemistry Department, National Research Center, El Bohouth St., Dokki, Giza 12622, Egypt



© The Author(s) 2025. **Open Access** This article is licensed under a Creative Commons Attribution 4.0 International License, which permits use, sharing, adaptation, distribution and reproduction in any medium or format, as long as you give appropriate credit to the original author(s) and the source, provide a link to the Creative Commons licence, and indicate if changes were made. The images or other third party material in this article are included in the article's Creative Commons licence, unless indicated otherwise in a credit line to the material. If material is not included in the article's Creative Commons licence and your intended use is not permitted by statutory regulation or exceeds the permitted use, you will need to obtain permission directly from the copyright holder. To view a copy of this licence, visit <http://creativecommons.org/licenses/by/4.0/>.

and energy harvesting [8, 10, 11, 20]. Also, combination of functionalized MOFs with different carbonaceous nanostructures creates effective sensing candidates for integrated electrochemical sensors [21–25].

Donepezil hydrochloride (DPH,  $\pm$ -2-[(1-Benzyl-4-piperidyl) methyl]-5,6-dimethoxy-1-indanone hydrochloride), is a reversible acetylcholinesterase enzyme (AChE) inhibitor which enhances the acetylcholine availability at the synapses with good communication among nerve cells and promoted cholinergic function [26, 27]. DPH has been administrated Alzheimer's dementia symptomatic treatment [27].

The official pharmacopoeial analytical approach for DPH based on chromatographic techniques [28]. However, different analytical approaches and research articles have been developed for measuring the DPH in biological fluids and pharmaceutical formulations [29]. Chromatographic techniques including HPLC–MS [30], HPLC–UV [31, 32], and diode-array (HPLC–DAD) [33] were the most common. Nevertheless, spectrofluorimetric and spectrophotometric measurements were also reported as an alternative choice for routine analysis of DPH in pharmaceutical forms [34–37]. Even though the aforementioned analytical approaches offer the required sensitivity and selectivity towards DPH; they are time-consuming with tedious analysis protocol and operate with high-cost instrumentations which obstacle their applications for high sample frequency and field monitoring of pharmaceutical residues in environmental samples. As a common and popular Alzheimer's medicine; developing of a new convenient and simple analytical method for determination of DPH residues is welcomed.

Electroanalytical measurements based on tailor-made electrochemical sensors possess the advantages of fast nondestructive measurement with low-cost equipment, [38]. Potentiometric sensors are considered as the most common and simple electrochemical sensors for monitoring of pharmaceutical residues [39–41]. The reported DPH potentiometric sensors were based on PVC membrane, solid-state, or carbon paste electrodes incorporated with either tetraphenylborate-DPH ion associates or cyclodextrin as electroactive materials [42–44]. However, these electrodes showed inherent limitations as they are too bulky with limited operational lifetimes and the requirement of sterilization for biomedical applications. As the consumption of pharmaceutical compounds continues to rise, disposable commercial sensors are adopted as a part of portable devices from “lab-to-market. Screen printing methodology is a common approach for commercialization of planner electrochemical sensors with high manufacturing reproducibility [45–49].

Molecular recognition through formation of inclusion complexes introduced alternative approaches for

enhancing the performance of the electrochemical sensors regarding their sensitivity and selectivity [50–53]. The effective attractive host–guest interactions forces included van der Waals forces,  $\pi$ – $\pi$  interaction, dipole–dipole, or hydrogen bonding. Among various macrocyclic compounds, cyclodextrins (CDs) were reported as the most popular sensing ionophores for electrochemical sensors. With a lipophobic interior cavity, CDs offer a suitable environment for fitting the guest molecule. The stability constants of the formed inclusion complexes are governed by the CD cavity size compatible with the guest molecule and the side substitution of the CD ring.

The present study aims to introduce cyclodextrins and other macrocyclic compounds including crown ethers, calixarenes, and their nanocomposites with metal organic frameworks as sensing element for potentiometric determination of DPH in the marketed pharmaceutical tablets and biological samples. Moreover, the presented sensors were introduced for monitoring the dissolution and degradation studies of DPH.

## Experimental

### Reagents and chemicals

All chemicals were analytical grade and bidistilled water (Milli-Q system, Millipore) was used in the present study. Different macrocyclic compounds, (supplied by Sigma-Aldrich), were tested as electroactive sensing elements including;  $\alpha$ -CD (I),  $\gamma$ -CD (II),  $\beta$ -CD (III), 2, 6-di-O-methyl- $\beta$ -CD (IV), 2, 3, 6-tri-O-methyl- $\beta$ -CD (V), 12-crown-4 ether (VI), 15-crown-5 ether (VII), 18-crown-6 ether (VIII), 21-crown-7 ether (IX), dibenzo-24-crown-8 ether (X), 30-crown-10 ether (XI), calix-4-arene (XII), and calix-8-arene (XIII).

The following tetraphenylborate derivatives were used as lipophilic additives in the sensing membrane, sodium tetraphenylborate (NaTPB, Fluka), potassium tetrakis (4-chlorophenyl) borate (KTCIPB, Fluka), and sodium tetrakis (4-fluorophenyl) borate (NaTFPB, Fluka). Tricresylphosphate (TCP, Fluka), dioctylsebacate (DOS, Avocado), dioctylphthalate (DOP, Sigma), *o*-nitro-phenyloctylether (*o*-NPOE, Sigma), and 2-fluorophenyl-2-nitrophenyl ether (*f*-PNPE, Fluka) were used as plasticizers.

Graphite powder and high molecular weight polyvinyl chloride (supplied by Aldrich) were applied for formulation of the homemade printing carbon ink and the sensing membrane matrix. Carbon nanotubes, either multiwall carbon nanotubes (MWCNTs, Aldrich) or single wall carbon nanotubes (SWCNTs, Aldrich) were used for synthesis of the nanocomposite with the cross-linked CD-MOFs complex.

### Authentic donepezil sample and the stock solution

Donepezil hydrochloride (DPH,  $C_{24}H_{29}ClNO_3$ , 379.49  $g\ mol^{-1}$ ) standard sample was obtained from the Arab Drug Company (ADCo, Cairo, Egypt). The stock drug solution ( $10^{-2}\ mol\ L^{-1}$ ) was prepared by dissolving a calculated amount of DPH authentic sample in water and kept in regenerator at 4 °C. Other DPH working solutions within the concentrations range from  $1 \times 10^{-3}$  to  $1 \times 10^{-7}\ mol\ L^{-1}$  were prepared by the serial dilution of the stock DPH solution.

### DPH pharmaceutical and biological samples

Donepezil pharmaceutical formulations (Aricept; 5 mg DPH/tablet; ADCo) were obtained from local markets. Five tablets were crushed to fine powder, dissolved in 50 mL water, and sonicated for 15 min. The DPH solution was filtrated and the drug content was assayed according to the pharmacopoeial protocol and the presented potentiometric sensor.

The standard plasma samples (purchased from VAC-SERA, Giza, Egypt) were enriched with known increments of the DPH stock solution, and mixed with acetonitrile (3:1 ratio). The fortified sample was centrifuged for 10 min to remove the residual sample protein. Urine sample were enriched with known aliquots of the stock DPH solution and mixed with equal volumes of methanol. The DPH contents in the clear supernatants were analyzed potentiometrically and according to the pharmacopoeial protocol.

### Measuring system

A portable Digital Multimeter with a PC interface (Radioshack, China) and 692-pH meter with a combined glass electrode (Metrohm, Switzerland) were used for potentiometric measurements and pH measurements, respectively. A single line flow injection system composed of four channels peristaltic pump (MCP Ismatec, Zurich, Switzerland), sample injection valve (ECOM, VentilC, Czech Republic), and home-designed continuous flow cells [54] was applied for flow injection analysis (FIA).

### Synthesis of metal organic framework- cross-linked macromolecule composite

#### Synthesis of Al MOF (MIL-53-NH<sub>2</sub>)

The amino functionalized MIL-53(Al) metal organic framework was synthesized and characterized as described in details elsewhere [17]. Briefly, the teflonlined stainless steel bomb filled with 28 mL water containing 0.120 g (0.66 mmol) of 2-amino-benzenedicarboxylic acid and 0.56 mL (0.22 mmol) of NaOH solutions were mixed with 1.10 mL (0.44 mmol)  $AlCl_3 \cdot 6H_2O$  solution. The reaction mixture was heated at 110 °C for 24 h to

complete the crystal growth. The formed MOF precipitate was washed several times with distilled water, DMF, soaked for 24 h in  $CH_2Cl_2$ , and dried at 80 °C.

**Preparation of MIL-53-NH<sub>2</sub>- cross-linked cyclodextrin composite** Two grams of the native  $\beta$ -CD was dissolved in 100 mL of acetic acid (2%) and mixed with 0.5 mL of epichlorohydrine at room temperature. The reaction mixture was kept at 60 °C for 4 h, incubated overnight at 50 °C, and the obtained solids were washed carefully to obtain pure cross linked cyclodextrin derivative.

Cyclodextrin-MOF composite was designed via post synthetic modification technique (Figure S1). The fresh cross-linked cyclodextrin was mixed with MIL-53-NH<sub>2</sub> in ultrasonic bath for about 2 h. The resultant solution was completed with another two hours in sonicated water bath keeping the MIL-53-NH<sub>2</sub> ratio at 20% from the total solid cyclodextrin content.

**Synthesis of MIL-53-NH<sub>2</sub>-cross-linked crown ether and calixarene composites** Selected other macromolecules, 18-crown-6 ether (VIII), and calix-8-arene (XIII), were cross-linked with the functionalized MIL-53(Al)-NH<sub>2</sub> as described in details elsewhere [17, 18].

### Construction of the disposable DPH sensors

The potentiometric-screen printed sensors were deposited on the PVC sheet using graphite and silver-silver chloride printing inks as described elsewhere [55]. The sensing membrane matrix was formulated by dissolving 2.0 mg of the MIL-53(Al)-NH<sub>2</sub>- $\beta$ -CD nanocomposite and 1.0 mg NaTFPB in 360 mg *f*-PNPE with continues stirring for 15 min. Next, 6 mL tetrahydrofuran, 240 mg PVC, and 15.0 mg MWCNTs were added and the sensing cocktail sonicated for 2 h. 20  $\mu$ L of the cocktail were drop-casted on the printed graphite/PVC track and left to dry for 24 h at 25 °C. The fresh fabricated sensors were preconditioned in  $10^{-3}\ mol\ L^{-1}$  DPH solution for 5 min before using.

### Measuring procedures

The constructed sensors were immersed in the measuring cell containing DPH solution within the ascending concentrations ranged from  $10^{-7}$  to  $10^{-2}\ mol\ L^{-1}$  at room temperature. The steady state potential values were plotted against the corresponding DPH concentration in logarithmic scale [56]. For FIA, 50  $\mu$ L of the authentic DPH solutions were injected in the carrier solution at the flow rate of 12.6  $mL\ min^{-1}$  and the electrode potential was monitored against time. The recorded peak heights were plotted against the corresponding DPH concentration [54].

### Analysis of samples

The contents of DPH in the marketed pharmaceutical formulation and biological fluids were assayed using the developed DPH disposable potentiometric sensors in comparison with the official procedures. Following the standard addition protocol, known aliquots of the stock DPH solution were mixed with the sample solution. For each increment, the steady state electrode potentials were measured and the DPH concentration in the sample solution was estimated [57].

For FIA measuring, 50  $\mu\text{L}$  of the DPH sample solution were injected in the carrier stream and the recorded peak height was compared with those recorded for injection of the standard DPH solutions of the same concentration.

The DPH samples containing 0.379 to 1.895 mg were potentiometrically titrated against the standardized NaTPB solution using the  $\beta$ -CD/MOF/MWCNTs/SPE as indicator electrode. After each addition, the steady state potential readings were recorded and plotted versus NaTPB volume. The end point was estimated from the first derivative of the sigmoid-shape titration curves [58].

### Donepezil tablet dissolution profile

One pharmaceutical tablet was put in the dissolution vessel filled with 50 mL of 0.1 mol HCl solution at 37 °C with a rotation speed 50 rpm [59]. After selected time intervals, 4 mL of the sample solution were withdrawn from the dissolution solution. The released DPH amounts in the dissolution medium were estimated spectrophotometrically at 271 nm and potentiometrically with the introduced DPH sensor [59, 60].

### Forced degradation studies of DPH

Different stress degradation protocols were applied to the authentic DPH sample. The stock DPH solutions (100  $\mu\text{g mL}^{-1}$ ), was undergone to thermal stress (70 °C), alkaline stress in NaOH solution, acidic hydrolysis in HCl solution, light exposure, and oxidative stress using  $\text{H}_2\text{O}_2$  solution at room temperature for seven days. The degradation process was followed using spectrophotometer at 271 nm at different time intervals [61].

## Results and discussion

### Characterization of the $\beta$ -CD- cross linked metal organic frameworks composite

SEM and TEM analysis described the morphological features of the synthesized samples. MIL-53- $\text{NH}_2$ - $\beta$ -CD exhibited cubic long strip structure with average diameter of sample was 84 nm (Fig. 1a, b).

The FTIR spectra of MIL-53- $\text{NH}_2$ ,  $\beta$ -CD, MIL-53- $\text{NH}_2$ - $\beta$ -CD are presented in Fig. 1c. MIL-53- $\text{NH}_2$  show the main characteristic bands of amino group, carboxylic group and benzene ring stretching at 3350, 1620–1505,

and 1404  $\text{cm}^{-1}$ , respectively.  $\beta$ -CD showed characteristic bands known as saccharides at 1640  $\text{cm}^{-1}$  (O–H bending vibration), 3400  $\text{cm}^{-1}$  (O–H stretching vibration), 2930  $\text{cm}^{-1}$  (C–H stretching vibration), and 1155  $\text{cm}^{-1}$  (C–O vibration).  $\alpha$ - Type glycosidic bond showed band located at 855  $\text{cm}^{-1}$ , which confirmed that CDs were consisted of glucopyranose units with  $\alpha$ -1, 4-glycosidic bond. The peak at 3400  $\text{cm}^{-1}$  was related to O–H stretching vibration.

FTIR spectrum of the cross-linked MIL-53- $\text{NH}_2$ - $\beta$ -CD composite showed the main characteristic bands of both MIL-53- $\text{NH}_2$  and  $\beta$ -CD. For confirming the composite (MIL-53- $\text{NH}_2$ -cross-linked  $\beta$ -CD), the changes in the intensity, shape and shift of the characteristic peaks can give considerable information about the chemical structure transformation. Peaks recorded for the cross-linked composite were wider than that of parent one, indicating hydroxypropyl groups incorporation broke the intramolecular hydrogen bond formed between C-2 and C-3. Moreover, the peak at 2960  $\text{cm}^{-1}$  corresponds to the anti-symmetric vibration of methylene groups.

XRD spectra were used to examine the crystalline skeleton of the MIL-53- $\text{NH}_2$  and MIL-53- $\text{NH}_2$ - $\beta$ -CD composites. Figure 1d shows the MIL-53- $\text{NH}_2$  and MIL-53- $\text{NH}_2$ - $\beta$ -CD composite XRD diffraction patterns. The compounds exhibits XRD peaks at  $2\theta$  values of 9.1°, 12.4°, 17.5°, 24.5°, 25.9°, 38.1°, and 44.6°, as shown in Fig. 00, which validates the structure of MIL-53- $\text{NH}_2$  [17]. The MIL-53- $\text{NH}_2$  and MIL-53- $\text{NH}_2$ - $\beta$ -CD composite's distinctive peaks are seen at the same angles, suggesting that MOF's crystalline structure does not change after  $\beta$ -CD impregnation. However, after modification with  $\beta$ -CD, the associated peaks widen, which is explained by the degree of crystallinity declining.

### Optimization of the sensing matrix

#### Nature of the sensing element

The electrode matrix was enriched with various macrocyclic compounds including cyclodextrin, crown ether, and calixarene derivatives (**I** to **XIII**). The blank electrodes, containing NaTPB as ionic sites, exhibited sub-Nernstian response values ( $42.2 \pm 2.2 \text{ mVdecade}^{-1}$ ) within a narrow linear DPH concentration range. Upon fortification with molecular recognition elements, improved potentiometric responses were recorded based on the nature of the sensing element (Fig. 2).

Among various cyclodextrin derivatives (Fig. 2a), the native  $\beta$ -CD (**III**) exhibited the proper Nernstian response ( $60.4 \pm 1.5 \text{ mVdecade}^{-1}$ ) within the DPH concentration ranged from  $10^{-6}$  to  $10^{-2} \text{ mol L}^{-1}$ . On the other hand, lower Nernstian responses ( $54.9 \pm 2.7$  and  $47.8 \pm 1.0 \text{ mVdecade}^{-1}$ ) were reported for both  $\alpha$ - and  $\gamma$ -CDs (**I**, **II**), respectively based their improper cavity



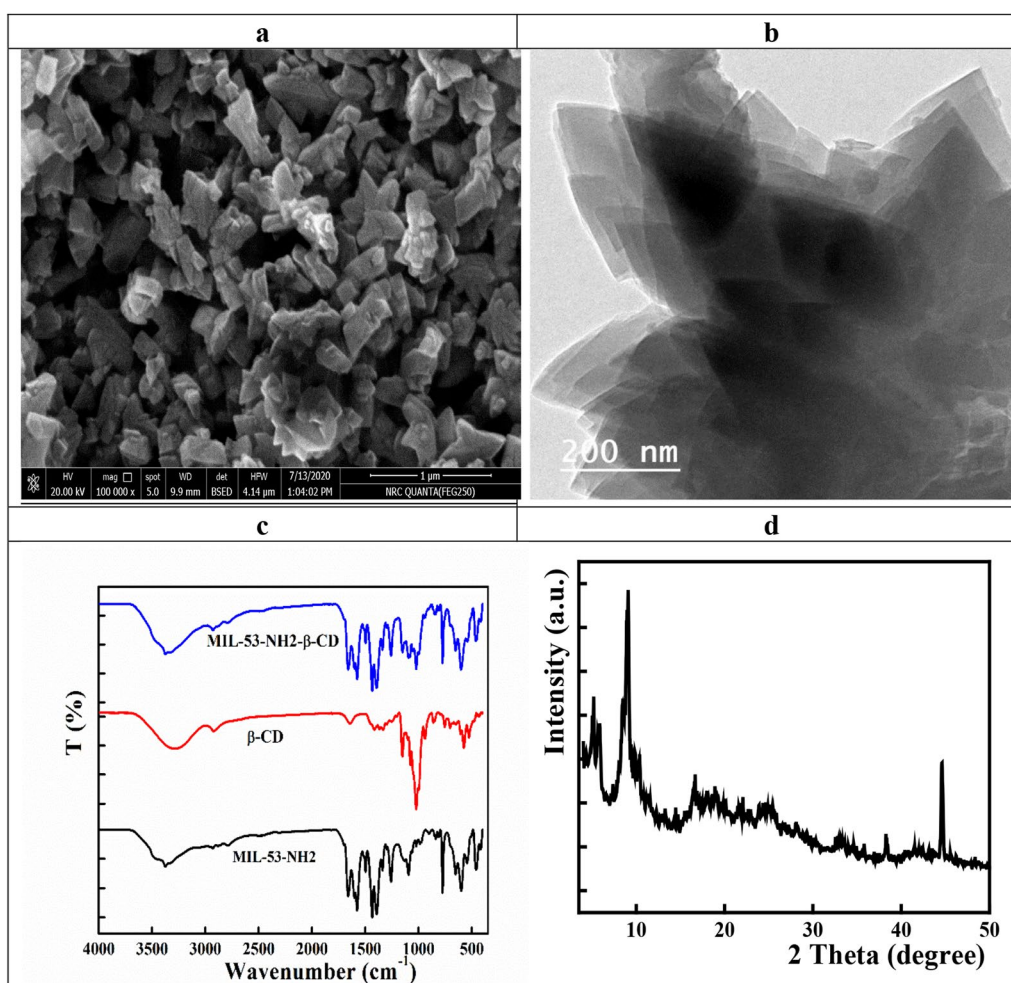


**Fig. 1** a SEM, b TEM, c FTIR, and d XRD of MIL-53-NH<sub>2</sub>-β-CD composite

size for fitting the DPH molecule. Side derivatization of the β-CD ring with the methyl groups (**IV**, **V**) showed slightly lower Nernstian response values with postulated steric hindrance. The lipophobic interior CD cavity offers a suitable environment for trapping the nonpolar part (aromatic benzene ring of the DPH molecule and formation of a stable inclusion complex. The stability constants of the formed inclusion complex are governed by the size of both CDs cavity, and the side substitution of the CD ring [50–53]. The postulated mechanism was illustrated in Figure S2.

Performing DPH potentiometric titration against NaTPB using the fabricated sensors as indicator electrodes, a similar trend was reported as β-CD (**III**) exhibited the highest total potential jump (311 mV) (Fig. 2b).

Crown ethers showed a conformation with a lipophobic cavity capable of fitting the guest molecule [50, 52]. The ring size relative to the guest molecule governed the stability constant of the formed CEs-DPH inclusion

complex. In the present study, the listed crown ethers recorded Nernstian slope values based their cavity size (Fig. 2c). Among them, 15-crown-5 ether (**VII**) and 18-crown-6 ether (**VIII**) showed the highest Nernstian responses ( $52.1 \pm 0.3$  and  $52.6 \pm 0.8$  mVdecade<sup>-1</sup>), compared to other crown ether derivatives with larger cavity size ( $47.8 \pm 2.3$  mV decade<sup>-1</sup> for 30-crown-10 ether **XI**). The same conclusion was recommended under potentiometric titration (Fig. 2d) suggesting crown ether (**VII**) as sensing ionophore.

Calixarenes are cavity-shaped cyclic oligomers made up of phenol units linked via alkylidene groups that can form host–guest inclusion complexes with a large variety of organic drug molecules [62]. In the present study, the performance of the sensors integrated with the selected β-CD (**III**), and crown ether (**VIII**), were compared with those containing calix-4-arene (**XII**), and calix-8-arene (**XIII**). The results indicated the superiority β-CD (**III**) compared with the other used ionophores under either

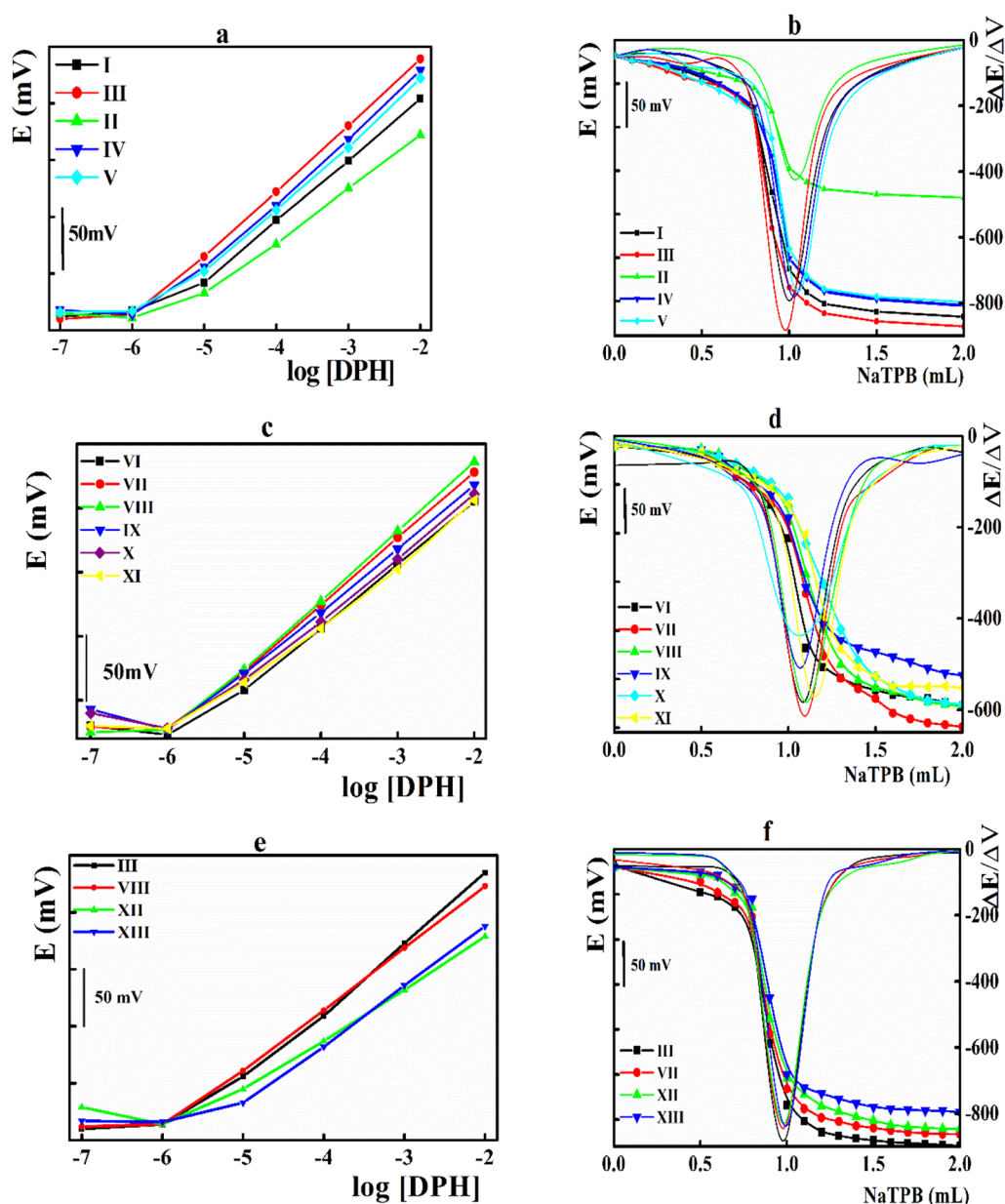


**Fig. 2** a, c, e Potentiometric behavior of the disposable sensors integrated with different sensing elements, and b, d, f potentiometric titration of DPH versus NaTPB solution applying the disposable sensors integrated with different sensing elements as indicator electrode

direct potentiometric or potentiometric titration measurements (Fig. 2e, f).

Next, the aforementioned selected sensing macromolecules were cross-linked with MIL-53-NH<sub>2</sub>, and the electrode matrix was enriched with the cross-linked compound instead of the free ionophore (Fig. 3). Noticeable enhancement of the electrode response upon cross-linking with the MOF was recorded based on the enhanced surface area and availability of more sensing sites. Integration of the electrode matrix with

β-CD-MOF composite showed the best performance under direct potentiometric and potentiometric titration measurements.

Nanomaterials, with their unique promising futures, enhance the electroactive surface area and the transduction of the possible chemical interaction to a measurable electrical signal within the electrode matrix, which improve the sensitivity of the sensor [1–6]. The potentiometric response of the printed sensors integrated with either the free β-CD or β-CD-MOF cross-linked

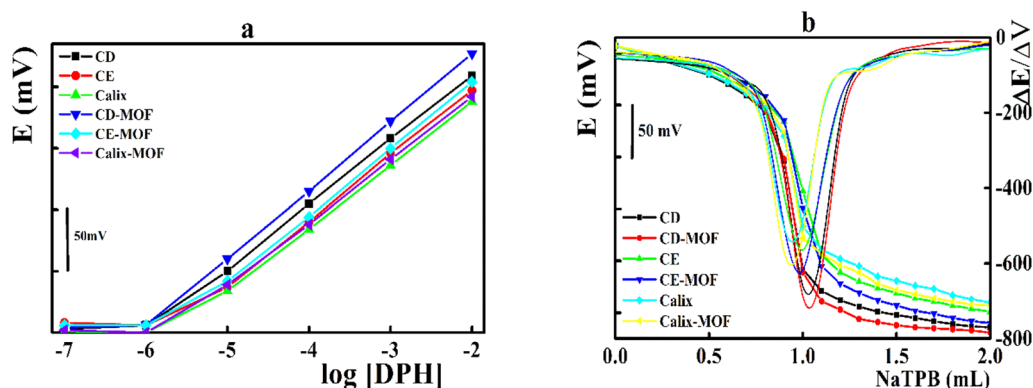


**Fig. 3** **a** Potentiometric behavior of the disposable sensors integrated with different sensing elements, **b** potentiometric titration of DPH versus NaTPB solution applying the disposable sensors integrated with different sensing elements as indicator electrodes

composites were evaluated in the presence of different carbonaceous nanomaterials such as MWCNTs and SWCNTs. Incorporation of MWCNTs improved the sensors performance with the highest Nernstian compliance  $58.5 \pm 0.6 \text{ mV decade}^{-1}$  and the total potential change under potentiometric titration mode (Fig. 4a, b).

Following the sensor fabrication protocol, the solid state nature required short preconditioning time

(the time required to record stable potential reading about  $\pm 1.0 \text{ mV}$  for the fresh electrode) compared with the PVC and liquid membrane electrodes. Moreover, incorporation of nanomaterials within the electrode matrix improves the hydrophobicity of the membrane surface which stabilized the electrode potential reading. Thus, sensors integrated with MWCNTs achieved potential stability reading within very short preconditioning

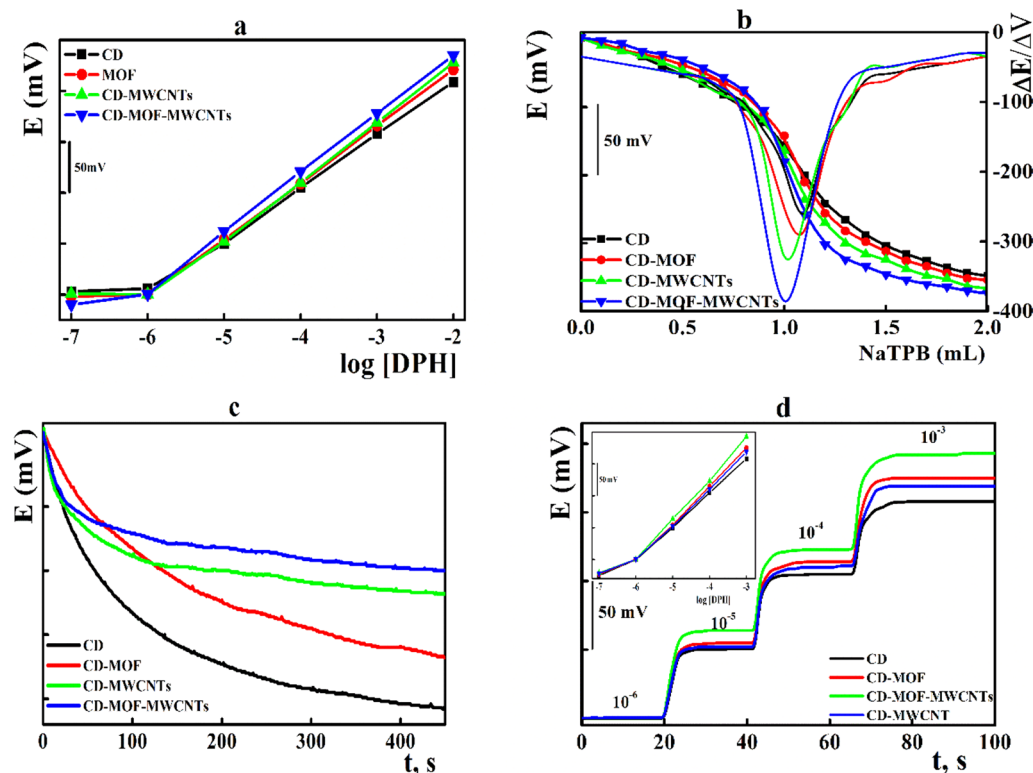


**Fig. 4** Influence of the sensing element on; **a** potentiometric response; **b** potentiometric titration of DPH versus NaTPB; **c** preconditioning time; **d** electrode response time

time (less than 5 min) compared with the corresponding carbon nanotube matrices (Fig. 4c).

For flow injection analysis and enzymatic reactions, the electrode response time (defined as the time required to attain 90% of the total potential jump after sudden tenfold increase in the analyte concentration) is usually questionable. The impact of the sensing element on the sensor response time was monitored within DPH concentration ranged from  $1 \times 10^{-6}$  to  $1 \times 10^{-3}$  molL<sup>-1</sup> (Fig. 4d). The fabricated sensors showed fast response time (ranged from 3 to 10 s), and the  $\beta$ -CD-MOF-MWCNTs based sensors were the best.

Next, the electrode matrix was enriched with different  $\beta$ -CD-MOF-MWCNTs content ranged from 0.0 to 5.0 mg. Ascending Nernstian slope values from  $42.2 \pm 2.2$  for the blank electrode to reach about  $56.0 \pm 0.3$  mV decade<sup>-1</sup> for 2.0 mg were recorded. Higher concentrations showed lower Nernstian slope values ( $52.3 \pm 0.9$  mV decade<sup>-1</sup> for 5.0 mg) due to the over saturation of the membrane matrix which hinder the complex formation between DPH and CD moiety.

#### Anionic sites effect

Cyclodextrins (CDs) behave as neutral carrier ionophores, therefore, cyclodextrin based sensors response only in the presence of charged ionic sites [63–65]. The presence of such ionic sites minimizes the sensing membrane resistance, enhances the ion exchange kinetics at the sensing membrane surface, and attracts the target analyte to the membrane surface for inclusion complex formation which improve the modified sensor selectivity and sensitivity.

Herein, the DPH performances characteristics of the sensors integrated with different tetraphenylborate derivatives and  $\beta$ -CD-MOF-MWCNTs as a promising sensing element were illustrated in Figure S3a. Improved sensitivities were recorded compared to the blank electrode, and NaTFPB showed the highest response (Nernstian response were  $30.8 \pm 0.5$ ,  $54.8 \pm 0.7$ ,  $60.6 \pm 0.4$ , and  $58.0 \pm 1.1$  mVdecade<sup>-1</sup> for the bare, NaTPB, NaTFPB, and KTCIPB, respectively). Potentiometric titration applying sensors fortified with different anionic sites sustained this concept as the highest potential jump was recorded in the presence of NaTFPB (Figure S3b).

#### Membrane plasticizer

The electroanalytical performance of the ionophore-based potentiometric sensors is mainly controlled by the membrane polarity, which is based on the dielectric constant value of the applied plasticizer. The membrane plasticizer governed the mobility of the sensing element and the formed inclusion complexes [65, 66]. For comparison, plasticizers having different dielectric constants

were used including; *f*-PNPE, *o*-NPOE, TCP, DOP, and DOS ( $\epsilon=50$ , 24.8, 17.6, 3.8, and 5.2, respectively) [67]. Sensor fabricated using high polar plasticizers showed ideal Nernstian slope values ( $60.1 \pm 0.4$  and  $60.7 \pm 1.5$  mVdecade<sup>-1</sup> for *o*-PNPE and *f*-NPOE, respectively) (Figure S4a).

Potentiometric titration measurements showed total potential jump and inflection at the end point related to the dielectrical constants of the aforementioned plasticizers [58]. The potential jump values were 165, 135, 118, 182, and 188 mV for TCP, DOS, DOP, *o*-NPOE and *f*-PNPE, respectively (Figure S4b).

#### Sensor performance

The performance characteristics of DPH sensors integrated with either free  $\beta$ -CD,  $\beta$ -CD-MOF or  $\beta$ -CD-MOF-MWCNTs as molecular recognition elements was evaluated following the IUPAC recommendation (Table 1) [56]. The  $\beta$ -CD-MOF-MWCNTs-based sensors showed the best performance with ideal Nernstian slope value of  $60.7 \pm 1.5$  mV decade<sup>-1</sup>, and low detection limit  $3 \times 10^{-7}$  molL<sup>-1</sup>.

Screen printing technique offers large-scale production of planner electrochemical sensors with high fabrication reproducibility. Herein, ten printed sensors showed average Nernstian slope value  $59.7 \pm 1.1$  mVdecade<sup>-1</sup>. Due to the absence of the internal reference solution and the solid nature of the fabricated sensors, prolonged lifetime about 24 weeks was achieved during which stable Nernstian responses ( $\pm 2$  mVdecade<sup>-1</sup>) was recorded. Moreover, the same fabricated disposable sensors can contentiously operate up to 4 weeks without loss of their performance.

The electroanalytical performance of the present DPH sensors was compared with the previously reported sensors [42–44]. The presented disposable sensors offer enhanced performance regarding their linear range, detection limit, fast response time, prolonged operational

**Table 1** Performance characteristics of various DPH screen-printed sensors

Parameter/sensing element	$\beta$ -CD	$\beta$ -CD-MOF	$\beta$ -CD-MOF-MWCNTs
Linear range (molL <sup>-1</sup> )	$10^{-6}$ – $10^{-2}$	$10^{-6}$ – $10^{-2}$	$10^{-6}$ – $10^{-2}$
Slope (mV decade <sup>-1</sup> )	$52.9 \pm 0.68$	$58.51 \pm 1.2$	$60.7 \pm 1.50$
R	0.9992	0.9990	0.9994
LOD (molL <sup>-1</sup> )	$1.0 \times 10^{-6}$	$7.0 \times 10^{-7}$	$3.0 \times 10^{-7}$
Response time (s)	10	8	3
Preconditioning time (min)	10	10	5
Shelf-life time (week)	4	12	24



lifetime and the possibility of miniaturization and commercialization (Table S1). Moreover, as the introduced sensors are disposable, relatively short preconditioning time was required with the advantages of mass production and high fabrication reproducibility.

For appropriate application of a developed potentiometric sensors, the working pH range is a crucial operating issue. The impact of the pH value on the potential response was monitored in a wide pH value ranged from 2 to 9 (Figure S5). Stable and reproducible electrode potentials were recorded within the pH ranged from 2 to 6 which are near the biological samples. At lower pH values, the sensor responses are severely influenced by  $H_3O^+$ , while at higher pH values, the electrode potential dramatically decreased due to the formation of un protonated DPH species (pKa value for DPH is 8.84).

### Selectivity and degradation studies

The sensor selectivity towards the excipients and additives present in the marketed pharmaceutical formulations is a crucial issue. The selectivity of a novel analytical approach reflects its ability to detect the target analyte in the coexistence of excipients and other interfering species. The selectivity of the potentiometric sensors was used to differentiate interfering species about target analyte by selectivity coefficient [68]. Usually, matched potential method (MPM) was more suitable to estimate the selectivity coefficient for the neutral compounds or different charged analytes [69]. Herein, the selectivity of the  $\beta$ -CD-MOF-MWCNTs based sensors against donepezil was promoted (Table 2) via inclusion complex formation between DPH molecule and cyclodextrin moiety within the nanocomposite structure.

Drug additives and the degradation profiling of a pharmaceutical compound mean the studying and quantifying of the various degradants in bulk materials. Detection and monitoring of those contaminants is the most crucial issues in the modern pharmaceutical industry. For a

newly introduced drug, the applied analytical techniques must be capable for monitoring of the parent active pharmaceutical compounds and degradants as recommended by ICH Guideline [59]. Moreover, some of the unidentified impurities and degradants formed during the shelf life may be health hazards, and therefore, identification and quantification of such impurities should be taken in consideration to show the safety of the final pharmaceutical product [70, 71].

The forced degradation studies were performed to provide adequate information to explore and identified the possible degradation pathways and formed degradants. Authentic donepezil material and commercial samples were exposed to forced and hydrolytic degradation studies [61]. Results indicated degradation of about 13% of DPH by refluxing in after 1 h an acidic medium, and 55% was degraded in the case of alkaline medium. On the other hand, oxidative stress degradation proceeded by degradation of 9% of the initial DPH with attacking of the electroactive amino group. Considering the thermal degradation and photolytic degradation of DPH, negligible degradation (<2%) was recorded. None of these degradation products exhibited noticeable interference in potentiometric titration of DPH against NaTPB. The reported interference and degradation studies devoted the application of the potentiometric approach for determination of DPH in the pharmaceutical samples as indicating method.

### Electroanalytical applications

#### Potentiometric titration

Potentiometric titration is one of the most efficient electroanalytical potentiometric tools with high accuracy and precision than the direct potentiometric mode which require calibrations of the measuring cells [58]. For potentiometric titration of DPH against NaTPB, the presented disposable sensors integrated with  $\beta$ -CD-MOF-MWCNTs nanocomposite showed sharp and reproducible titration curves ( $\Delta E$  values ranged from 196 to 264 mV) within DPH concentration ranged from 0.379 to 1.895 mg (Fig. 5 a). Moreover, high reproducibility with total average recovery of  $100.5 \pm 2.51\%$  was recorded when titrating of 0.379 mg DPH (Fig. 5 b).

**Flow injection analysis** Due to its high sampling frequency, and improved reproducibility, potentiometric sensors were incorporated as a detector in flow injection systems [72]. Both the response time and the linearity range of the potentiometric sensor controlled its behavior in flow injection systems [73]. Herein, the modified DPH sensor showed stable potential readings which in turn decrease the FIA peak residence time and increased the sampling output up to 90 samples  $h^{-1}$ . Calibration

**Table 2** Potentiometric selectivity coefficients-of the  $\beta$ -CD-MOF-MWCNTs integrated sensors

Interferent	$-\log K_{A,B}$	Interferent	$-\log K_{A,B}$
$Li^+$	3.80	Maltose	3.90
$NH_4^+$	3.40	Starch	3.74
$Ca^{2+}$	3.10	Sucrose	3.60
$Mg^{2+}$	3.44	Glucose	3.29
$Ni^{2+}$	3.90	Fructose	3.35
$Co^{2+}$	3.53	Glycine	2.85
Phosphate	3.70	Caffeine	3.40
Citrate	2.54	Cysteine	2.80

<sup>a</sup> Lower and upper concentrations of DPH,  $10^{-5}$  and  $10^{-2}$  molL<sup>-1</sup> respectively

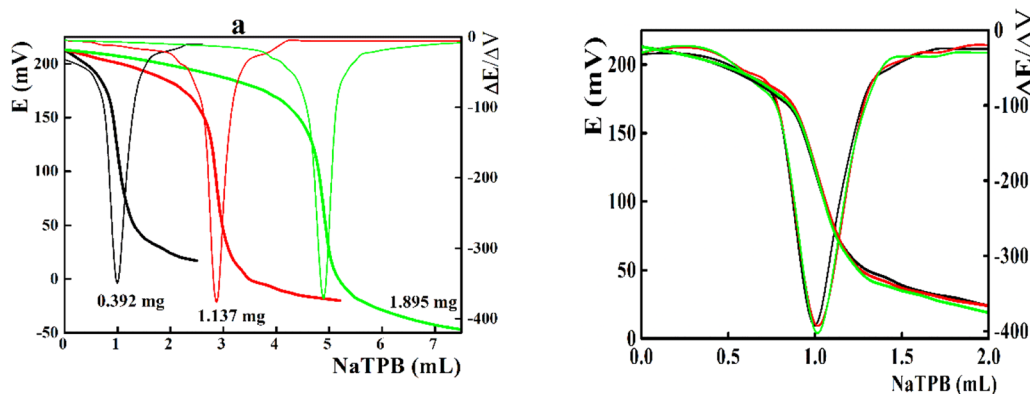


**Fig. 5** **a** Potentiometric titration of DPH against NaTPB using  $\beta$ -CD-MOF-MWCNTs based sensors, and **b** titration reproducibility for 0.392 mg DPH against NaTPB

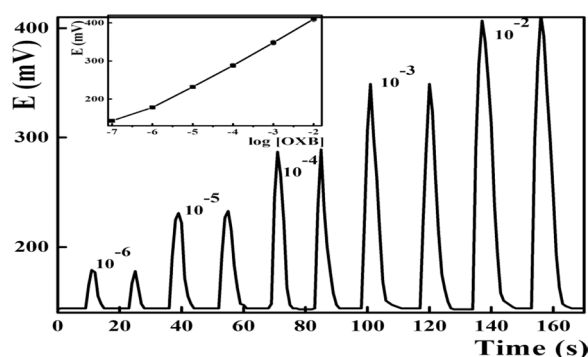


**Fig. 6** FIA potentiometric analysis of DPH with  $\beta$ -CD-MOF-MWCNTs based sensors

graphs (Fig. 6) were illustrated via injection of 50  $\mu$ L DPH authentic solution in the carrier stream covering the DPH concentration range from  $10^{-6}$  to  $10^{-2}$  mol L $^{-1}$  with Nernstian response of  $61.0 \pm 1.1$  mVdecade $^{-1}$ .

**Sample analysis** Based on the recorded satisfactory improved sensitivity and selectivity, the modified sensors can be encouraged as a suitable tool for DPH analysis in various biological and pharmaceutical samples under direct potentiometric measurement, potentiometric titration and flow injection modes. As tabulated in Table 3, satisfactory agreement was achieved for DPH in various samples using the modified sensor and official methods (Table 3).

**Dissolution behavior of DPH pharmaceutical tablet** Studying the absorption of the pharmaceutical active ingredient after the oral administration represents a crucial factor to explore the drug pharmacokinetics behavior and the active material release from the drug formulations and its entrance through the gastro-intestinal tract. More-

over, the in vitro dissolution studies are usually relevant to show the in vivo performance and drug product bio-availability, and finally, observing novel formulations that might have slower or faster release rate.

Recently, electrochemical sensors have been employed for the in-line analysis of dissolution studies [74–76]. The present work described the dissolution profiles of donepezil in the commercial pharmaceutical sample where the DPH released in the dissolution medium was monitored using the developed DPH sensor and the UV-spectrophotometric measurements at 271 nm. Results illustrated in Figure S6 confirmed the agreement in recoveries recorded by both techniques ( $\pm 3.0\%$ ). As a result, releasing of DPH was reported to be rapid (90% amount of DPH was released within 15 min) and complete after 30 min.

## Conclusions

The present study introduces the construction and electroanalytical validation of novel donepezil printed potentiometric sensors based on  $\beta$ -cyclodextrin cross-linked metal organic framework-multiwall carbon nanotube composite as recognition element. The  $\beta$ -CD-MOF-MWCNTs based sensors exhibit Nernstian compliance value of  $60.7 \pm 1.5$  mV decade $^{-1}$  and fast response time about 3 s and long lifetime about 24 weeks within the DPH concentration ranged from  $10^{-6}$  to  $10^{-2}$  mol L $^{-1}$ . The proposed planner sensor can be introduced for routine analysis of DPH in various samples, and monitoring of the degradation process and dissolution profile. The modified sensors show improvement in electroanalytical characteristics compared with the previously reported DPH sensors regarding their sensitivity, response time, dissolution and degradation mentoring, FIA and potentiometric titration measurements.

**Table 3** Potentiometric determination of DPH in the marketed pharmaceutical formulations and biological samples

Sample	Taken (µg)	Aricept®			Spiked urine			Spiked Plasma		
		Found (µg)	Recovery	RSD	Found (µg)	Recovery	RSD	Found (µg)	Recovery	RSD
Standard addition	3.79	3.823	100.87	1.7	3.615	95.3	3.4	3.64	96.2	2.6
	37.9	37.83	95.23	1.2		96.4	2.0	35.5	93.88	3.3
	379	372.30	98.23	1.9		97.0	2.2	358	94.46	1.9
Titration	379	360.05	95.0	1.4	348.68	92.0	3.7	347	91.55	3.6
	1137	1108.6	97.5	2.0	1091.5	90.0	3.0	1074.5	94.5	3.4
	1895	1847.7	97.8	1.5	1828.7	96.5	1.8	1790.8	94.5	2.7
FIA	3.79	3.845	101.45	1.55						
	37.9	38.21	100.81	1.82						
	379	374.15	98.70	1.88						

<sup>a</sup> Mean recovery and relative standard deviations of three determinations

## Abbreviations

DPH	Donepezil hydrochloride
$\beta$ -CD	$\beta$ -Cyclodextrin
MOFs	Metal frame works
MWCNTs	Multi wall carbon nanotubes
SWCNTs	Single wall carbon nanotubes
FIA	Flow injection analysis
LOD	Limit of detection
PVC	Polyvinyl chloride
NaTPB	Sodium tetraphenylborate
NaTFPB	Sodium tetrakis (4-fluorophenyl) borate
KTCIPB	Potassium tetrakis (4-chlorophenyl) borate
DOS	Diocetylsebacate
DOP	Diocetylphthalate
TCP	Tricresylphosphate
o-NPOE	o-Nitro-phenyloctylether
f-PNPE	2-Fluorophenyl-2-nitrophenyl ether
DMF	Dimethyl formamide
SEM	Scan electron microscopy
TEM	Transmission electron microscopy
XRD	X-ray diffraction
FTIR	Fourier transform infrared spectroscopy

## Supplementary Information

The online version contains supplementary material available at <https://doi.org/10.1186/s13065-025-01521-2>.

Supplementary material 1.

## Acknowledgements

Authors acknowledge the support from the project 13020205 NRC (National Research Center).

## Author contributions

Rehab O. El-Attar: collect information, methodology, preparation figures, writing—review & editing. Reda M. Abdelhameed: resources, formal analysis, methodology, writing—review & editing. Elmorsy Khaled: preparation figures, data curation, supervision, writing—review & editing.

## Funding

Open access funding provided by The Science, Technology & Innovation Funding Authority (STDF) in cooperation with The Egyptian Knowledge Bank (EKB). Open access funding provided by the Science & Technology & Innovation Funding Authority (STDF) in cooperation with the Egyptian Knowledge Bank (EKB).

## Availability of data and materials

No datasets were generated or analysed during the current study.

## Declarations

### Ethics approval and consent to participate

Not applicable.

### Consent for publication

Not applicable.

### Competing interests

The authors declare no competing interests.

Received: 18 October 2024 Accepted: 16 May 2025

Published online: 29 May 2025

## References

- Yin T, Qin W. Applications of nanomaterials in potentiometric sensors. *TrAC, Trends Anal Chem.* 2013;51:79–86.
- Brainina K, Stozhko N, Bukharinova M, Vikulova E. Nanomaterials: electrochemical properties and application in sensors. *Phys Sci Rev.* 2018. <https://doi.org/10.1515/psr-2018-8050>.
- Kurbanoglu S, Ozkan SA, Merkoçi A. Electrochemical nanobiosensors in pharmaceutical analysis. *Novel Dev Pharm Biomed Anal.* 2018;2:302–53.
- Falola TO. Nanoparticles modified electrodes: synthesis, modification, and characterization—review. *World J Nano Sci Eng.* 2022;12:29–62.
- Manjunatha C, Khosla A, Krishna RH, Ashoka S. Current progress in materials, device fabrication, and biomedical applications of potentiometric sensor devices: a short review. *ECS Trans.* 2022;107(1):6343.
- Qian L, Durairaj S, Prins S, Chen A. Nanomaterial-based electrochemical sensors and biosensors for the detection of pharmaceutical compounds. *Biosen Bioelectron.* 2021;175:112836.
- Batten SR, Neville SM, Turner DR. Porous coordination polymers, Chapter 10. In: *coordination polymers: design*. Cambridge: The Royal Society of Chemistry; 2009. p. 313–44.
- Kumar P, Deep A, Kim KH. Metal organic frameworks for sensing applications. *TrAC, Trends Anal Chem.* 2015;73:39.
- Wang Z, Cohen SM. Post synthetic modification of metal–organic frameworks. *Chem Soc Rev.* 2009;38(5):1315–29.
- Furukawa H, Cordova KE, O’Keeffe M, Yaghi OM. The chemistry and applications of metal–organic frameworks. *Science.* 2013;341(6149):1230444.
- Zhu QL, Xu Q. Metal–organic framework composites. *Chem Soc Rev.* 2014;43(16):5468–512.
- Wang S, Mc Guirk CM, d’Aquino A, Mason JA, Mirkin CA. Metal–organic framework nanoparticles. *Adv Mater.* 2018;30(37):1800202.
- Hartlieb KJ, Peters AW, Wang TC, Deria P, Farha OK, Hupp JT, Stoddart JF. Functionalised cyclodextrin-based metal–organic frameworks. *Chem Commun.* 2017;53(54):7561–4.
- He Y, Hou X, Liu Y, Feng N. Recent progress in the synthesis, structural diversity and emerging applications of cyclodextrin-based metal–organic frameworks. *J Mater Chem B.* 2019;7(37):5602–19.
- Roy I, Stoddart JF. Cyclodextrin metal–organic frameworks and their applications. *Acc Chem Res.* 2021;54(6):1440–53.
- Dummert SV, Saini H, Hussain MZ, Yadava K, Jayaramulu K, Casini A, Fischer RA. Cyclodextrin metal–organic frameworks and derivatives: recent developments and applications. *Chem Soc Rev.* 2022;51(12):5175–213.
- El-Attar RO, Abdelhameed RM, Khaled E. Synthesis and applications of crown ether-linked metal–organic framework composite-based sensors for stripping voltammetric determination of lead. *Arab J Sci Eng.* 2024;49(1):637–47.
- El-Attar RO, Shoukry EM, Mohamed EF, Omran S, Khaled E. Macromolecules cross linked-metal organic frame works based sensors for determination of memantine hydrochloride. *Egypt J Chem.* 2023;66(13):2059–71.
- Tan Q, Chen C, Lin C, Zhang J, Liu S, Zhang J. Highly sensitive detection of kaempferol using electrochemical sensors based on 3D-ordered mesh interconnect C60-GO, Ni-MOF, and  $\beta$ -cyclodextrin. *Microchem J.* 2024;197:109866.
- Mohan B, Kumar S, Kumar A, Kumar K, Modi K, Jiao T, Chen Q. Analogize of metal–organic frameworks (MOFs) adsorbents functional sites for  $Hg^{2+}$  ions removal. *Sep Purif Technol.* 2022;297:121471.
- Liu W, Yin XB. Metal–organic frameworks for electrochemical applications. *TrAC, Trends Anal Chem.* 2016;75:86–96.
- Xu Y, Li Q, Xue H, Pang H. Metal–organic frameworks for direct electrochemical applications. *Coord Chem Rev.* 2018;376:292–318.
- Liu L, Zhou Y, Liu S, Xu M. The applications of metal–organic frameworks in electrochemical sensors. *Chem Electro Chem.* 2018;5(1):6–19.
- Fang X, Zong B, Mao S. Metal–organic framework-based sensors for environmental contaminant sensing. *Nano-micro letters.* 2018;10:1–19.
- Zaimbashi R, Salarizadeh N, Askari MB. Electrochemical sensor based on Ni-Co-MOF/MWCNTs nanocomposite and benzoyl ferrocene for determination of L-cysteine in the presence of tryptophan. *Inorg Chem Commun.* 2025;171:113403.
- Sugimoto H, Ogura H, Arai Y, Iimura Y, Yamanishi Y. Research and development of donepezil hydrochloride, a new type of acetylcholinesterase inhibitor. *Jap J Pharmacol.* 2002;89(1):7–20.
- Barner EL, Gray SL. Donepezil use in Alzheimer disease. *Annal Pharmacol.* 1998;32(1):70–7.



28. USP Monograph. Donepezil hydrochloride, USP35-NF30. The United States Pharmacopeial Convention, Official from. 2012.
29. Asiri YA, Mostafa GA. Donepezil. In: Profiles of drug substances, excipients and related methodology. Cambridge: Academic Press; 2010. p. 117–50.
30. Jeong HC, Park JE, Hyun JY, Park MK, Shin DS, Shin KH. Determination of donepezil in human plasma using ultra performance liquid chromatography-tandem mass spectrometry. *Translat Clinical Pharmacol*. 2018;26(2):64.
31. Yasui-Furukori N, Furuya R, Takahata T, Tateishi T. Determination of donepezil, an acetylcholinesterase inhibitor, in human plasma by high-performance liquid chromatography with ultraviolet absorbance detection. *J Chromatogr B*. 2002;768(2):261–5.
32. Nakashima K, Itoh K, Kono M, Nakashima MN, Wada M. Determination of donepezil hydrochloride in human and rat plasma, blood and brain micro dialysates by HPLC with a short C30 column. *J Pharma Biomed Anal*. 2006;41(1):201–6.
33. Petrocheilou M, Samanidou V, Kovatsi L, Tsolaki M, Papadopoulos I. A simple and direct HPLC-DAD method for the simultaneous determination of galantamine, donepezil and rivastigmine in cerebrospinal fluid, blood serum and urine. *J Appl Bioanal*. 2017;3(4):1847.
34. Abbas SS, Fayed YM, Fattah LESA. Stability indicating methods for determination of donepezil hydrochloride according to ICH guidelines. *Chem Pharm Bull*. 2006;54(10):1447–50.
35. Patel C, Patel N, Kothari C. Quantitative determination of donepezil hydrochloride by a simple and accurate synchronous spectrofluorimetric method in human plasma. *J Young Pharm*. 2014;6(4):47.
36. Sangshetti JN, Mahapare PR, Paramane S, Shinde DB. Spectrophotometric estimation of donepezil hydrochloride in bulk and tablet formulation. *Trends Appl Sci Res*. 2008;3(1):109–12.
37. Shirwaikar A, Devi S, Rajagopal PL, Kiron SS, Sreejith KR. Development and validation of analytical method for determination of donepezil hydrochloride in pure and dosage forms. *Asian J Pharm Clin Res*. 2014;7(1):149–53.
38. Siddiqui MR, Al Othman ZA, Rahman N. Analytical techniques in pharmaceutical analysis: a review. *Arab J Chem*. 2017;10:51409–21.
39. Özbek O, Berkel C, Isildak Ö. Applications of potentiometric sensors for the determination of drug molecules in biological samples. *Crit Rev Anal Chem*. 2022;52(4):768–79.
40. Mostafa IM, Meng C, Dong Z, Lou B, Xu G. Potentiometric sensors for the determination of pharmaceutical drugs. *Anal Sci*. 2022;38(1):23–37.
41. Jadon N, Hosseinzadeh B, Kaya SI, Ozelikay-Akyildiz G, Cetin Kaya A, Ozkan SA. Emerging trends of ion-selective electrodes in pharmaceutical applications. *Electrochim Acta*. 2024;488:144204.
42. Mostafa GAH, Hefnawy M, Al-Majed A. Membrane sensors for the selective determination of donepezil hydrochloride. *J AOAC Inter*. 2010;93(2):549–55.
43. Rajendraprasad N. Highly selective sensors for assay of donepezil hydrochloride by potentiometry: green approaches. *Anal Bioanal Electrochem*. 2021;13(1):33–51.
44. Khamees N, Mohamed TAF, Derar AR, Aziz A. All-solid-state, PVC membrane, and carbon paste ion-selective electrodes for determination of donepezil hydrochloride in pharmaceutical formulation. *J AOAC Int*. 2017;100(5):1414–9.
45. Mohamed HM. Screen-printed disposable electrodes: Pharmaceutical applications and recent developments. *TrAC Trends in Anal Chem*. 2016;82:1–11.
46. Ambaye AD, Kefeni KK, Mishra SB, Nxumalo EN, Ntsendwana B. Recent developments in nanotechnology-based printing electrode systems for electrochemical sensors. *Talanta*. 2021;225:121951.
47. Ferrari AGM, Rowley-Neale SJ, Banks CE. Screen-printed electrodes: transitioning the laboratory in-to-the field. *Talanta Open*. 2021;3:100032.
48. Singh S, Wang J, Cinti S. An overview on recent progress in screen-printed electroanalytical (bio) sensors. *ECS Sens Plus*. 2022;1:023401.
49. Crapnell RD, Banks CE. Electroanalytical overview: screen-printed electrochemical sensing platforms. *Chem Electro Chem*. 2024;11:202400370.
50. Ganjali MR, Norouzi P, Rezapour M, Faridbod F, Pourjavid MR. Supramolecular based membrane sensors. *Sensors*. 2006;6:1018–86.
51. Shahgaldian P, Pielas U. Cyclodextrin derivatives as chiral supramolecular receptors for enantioselective sensing. *Sensors*. 2006;6:593–615.
52. Faridbod F, Ganjali MR, Dinarvand R, Norouzi P, Riahi S. Schiff's bases and crown ethers as supramolecular sensing materials in the construction of potentiometric membrane sensors. *Sensors*. 2008;8:1645–1073.
53. Lenik J. Cyclodextrins based electrochemical sensors for biomedical and pharmaceutical analysis. *Curr Med Chem*. 2017;24(22):2359–91.
54. Khaled E, Hassan HNA, Mohamed GG, Seleim AEA. Towards disposable sensors for drug quality control: dextromethorphan screen printed electrodes. *Drug Test Anal*. 2010;2(9):424–9.
55. Khaled E, Kamel MS, Hassan HNA, Abdel-Gawad H, Aboul-Enein HY. Performance of a portable biosensor for the analysis of ethion residues. *Talanta*. 2014;119:467–72.
56. Buck RP, Lindner E. Recommendations for nomenclature of ion selective electrodes. *Pure Appl Chem*. 1994;66:2527–36.
57. Baumann EW. Trace fluoride determination with specific ion electrode. *Anal Chim Acta*. 1968;42:127–32.
58. Vytrās K. Potentiometric titrations based on ion-pair formation. In: Ion-selective electrode reviews, vol. 7. Amsterdam: Elsevier; 1985. p. 77–164.
59. ICH Q1A guideline. International Conference on Harmonisation (ICH); Stability Testing of New Drugs Substances and Products, Q1A (CPMP/ICH/2736/99), Geneva, 1999.
60. De Campos DP, Silva-Barcellos NM, Marinho FDM, Barbosa GX, Lana VLVV, de Souza J. A sustainable UPLC-UV method for quantification of donepezil hydrochloride in biorelevant media applied to dissolution profile comparison. *Drug Dev Ind Pharm*. 2020;46(10):1578–88.
61. Ruela AL, Santos MG, Figueiredo, EC Pereira, GR, LC-PDA and LC-MS studies of donepezil hydrochloride degradation behaviour in forced stress conditions. *J Braz Chem Soc*. 2014;25:2094–101.
62. Lo PK, Wong MS. Extended calix [4] arene-based receptors for molecular recognition and sensing. *Sensors*. 2008;8:5313–35.
63. Schaller U, Bakker E, Pretsch E. Carrier mechanism of acidic ionophores in solvent polymeric membrane ion-selective electrodes. *Anal Chem*. 1995;67(18):3123–32.
64. Schaller U, Bakker E, Spichiger UE, Pretsch E. Ionic additives for ion-selective electrodes based on electrically charged carriers. *Anal Chem*. 1994;66(3):391–8.
65. Bakker E, Bühlmann P, Pretsch E. Polymer membrane ion selective electrodes—what are the limits? *Electroanal Int J Devoted Fundamental Pract Aspects Electroanal*. 1999;11(13):915–33.
66. Vytrās K, Kalous J, Jezkova J. Automated potentiometry as an ecologic alternative to two-phase titrations of surfactants. *Egypt J Anal Chem*. 1997;6(1):107–23.
67. Visser HC, de Jong F, Reinhoudt DN. Kinetics of carrier-mediated alkali cation transport through supported liquid membranes: effect of membrane solvent, co-transported anion, and support. *J Membr Sci*. 1995;107(3):267–76.
68. Umezawa Y. Ion selective electrodes. In: Encyclopedia of supramolecular chemistry, vol. 2. Boca Raton: CRC Press; 2013. p. 747–52.
69. Tohda K, Dragoe D, Shibata M, Umezawa Y. Studies on the matched potential method for determining the selectivity coefficients of ion-selective electrodes based on neutral ionophores: experimental and theoretical verification. *Anal sci*. 2001;17(6):733–43.
70. Görög S. Critical review of reports on impurity and degradation product profiling in the last decade. *TrAC Trends Anal Chem*. 2018;101:2–16.
71. Jain D, Basniwal PK. Forced degradation and impurity profiling: recent trends in analytical perspectives. *J Pharm Biomed Anal*. 2013;86:11–35.
72. Trojanowicz M, Szewczynska M, Wcislo M. Electroanalytical flow measurements—recent advances. *Electroanal Inter J Devoted Fund Pract Aspects Electroanal*. 2003;15(5–6):347–65.
73. Khaled E, Kamel M, Hassan H. Comparison of detectors and cell configurations in flow-injection potentiometric technique of pharmaceutical analysis original paper. *J Flow Injec Anal*. 2010;27(1):20.
74. Bohets H, Vanhoutte K, De Maesschalck R, Cockaerts P, Vissers B, Nagels LJ. Development of in situ ion selective sensors for dissolution. *Anal Chim Acta*. 2007;581(1):181–91.
75. Khaled E, El-Sabbagh IA, El-Kholy NG, Ghahni EA. Novel PVC-membrane electrode for flow injection potentiometric determination of Biperiden in pharmaceutical preparations. *Talanta*. 2011;87:40–5.
76. Elzanfaly ES, Hassan SA, Salem MY, El-Zeany BA. In-line potentiometric monitoring of dissolution behavior of verapamil hydrochloride versus traditional pharmacopeial method: a comparative study. *Sens Actua B Chem*. 2016;228:587–94.

## Publisher's Note

Springer Nature remains neutral with regard to jurisdictional claims in published maps and institutional affiliations.